MINERALOGICAL MAGAZINE, SEPTEMBER 1978, VOL. 42, PP. 373-82

Glauconite and celadonite: two separate mineral species

H. A. BUCKLEY, J. C. BEVAN, K. M. BROWN, AND L. R. JOHNSON
Department of Mineralogy, British Museum (Natural History), Cromwell Road, London SW7 5BD
AND
V. C. FARMER
The Macaulay Institute for Soil Research, Craigiebuckler, Aberdeen AB9 2QJ

SUMMARY. Analyses of glauconites and celadonites from continental sedimentary rocks and sea-floor basalts using X-ray diffraction, electron probe microanalysis, infra-red spectroscopy, and X-ray fluorescence spectroscopy are reported. The minerals are shown to be distinct species; each an isomorphous replacement series, glauconite having an average half unit cell of $K_{0.85}(Fe^{3+}, Al^{3+})_{1.34}(Mg^{2+}, Fe^{2+})_{0.66}(Si_{3.76}Al_{0.24})O_{10}(OH)_2$ whereas celadonite approaches the ideal half unit cell of $K(Fe^{3+}, Al^{3+})(Mg^{2+}, Fe^{2+})Si_4O_{10}(OH)_2$. Considerable Fe^{3+}–Al^{VI} interchangeability occurs in the octahedral layer in both minerals and considerable substitution of aluminium in the tetrahedral layer of glauconites results in the more disordered 1*Md* type of structure compared with the more highly ordered 1*M* structure of celadonites. Some mixed layer glauconite–smectites and celadonites were also examined and could be distinguished from true glauconites and celadonites by chemical analysis, XRD, and IR techniques. It is proposed that the terms 'glauconite' and 'celadonite' should be used only for those minerals containing less than 5% interlayering.

CONTROVERSY over the structure, composition, and terminology of glauconite and celadonite has existed for decades. It is well established that both are iron-rich, hydrous silicates with a dioctahedral structure, within which considerable chemical variations can occur. Although the two minerals are found in widely differing environments, glauconite occurring in recent and fossil sediments and celadonite in altered volcanic rocks, they are considered by some authors (Foster, 1969) to form an isomorphous replacement series. This paper deals with the identification and characterization of the pure mineral species.

A major problem in clay analysis is sample purity; for classical wet chemical techniques, the size of the sample invariably precludes removal of trace amounts of other minerals. This paper records the analyses of both minerals using X-ray diffraction (XRD), infra-red spectrometry (IR), electron probe microanalysis (EPMA), and X-ray fluorescence (XRF). Modern XRD and IR techniques analyse a relatively large sample compared with EPMA; they do, however, distinguish and identify most of the minerals present. Since the areas of individual analysis by EPMA approach 1 μm in diameter, most impurities can be avoided by using this technique. The external morphology of selected samples was determined using a Cambridge Instruments' 600 Stereoscan.

Sample selection and preparation. Fifty-seven glauconite and twenty-five celadonite samples were examined initially by XRD and those containing greater than 5% interstratification or other impurities were rejected. Twenty-six glauconites and twenty celadonites were then selected for further investigation by IR while eighteen of the glauconites and fifteen of the celadonites were analysed by EPMA. The glauconites came from a wide variety of localities: land outcrops, boreholes, and submarine continental shelf deposits (Table I). The celadonites came from ocean-floor basalts and continental volcanic rocks (Table II).

The glauconite was separated from the host rock by gentle crushing followed by cleaning in an ultrasonic bath. There have been many descriptions of the various types of glauconitic pellets found in rocks (e.g. McRae, 1972): in the present work only two distinctions are made. Most of the glauconite is in the form of dark green pellets 100–1000 μm in size, which bear the suffix 'D' in Tables I and III. A much rarer form occurs as light green lumps (suffix 'L' in Table I), which lack the typical pelletal form and from their external morphology appear to have formed subsequent to the 'D' pellets, since they bear the impressions of adjoining mineral grains.

TABLE I. *Location, description, and analysis of glauconite samples*

Geological horizon and locality	Description	No.	XRD analysis	IR analysis
Lower Greensand				
Probably Gault/Lower Greensand junction beds, Glyndebourne Bore BDK 4128*, Sussex	olive green pellets	1L	g, cl, q	g, i, q
Folkestone Beds, Oxney Bore K544*, 835 ft, Kent	dark green pellets	5D	g, m, c, q, go	diffuse, c
	rare light green lumps	na		
Probably Gault/Lower Greensand junction beds, Oxney Bore Bw 1720*, 805 ft, Kent	light green massive	4L	g, cl	g
Gault/Lower Greensand junction beds, Dover Bore, BM. 1905, 202, Dover, Kent	large light green lumps	7L	g	g, c, q, i
	small dark green pellets	7D	g, c	g, c
	large light green lumps	—	g stained pebbles	
	botryoidal dark green lumps	—	apatite with g	
Folkestone Stone Beds, Copt Point, Folkestone, Kent	dark green pellets	8D	g, cl	g, q
	light green lumps	8L	g, cl	g, q, i
Folkestone Beds, 20 ft below base of Gault, Copt Point, Folkestone, Kent	large light green lumps	9L	g, cl, q, p	g, i, q
	large dark green lumps	9D	g, cl	g, q
Folkestone Beds, 1 ft below base of Gault, Copt Point, Folkestone, Kent	dark green pellets	11D	g	g
	rare light green lumps	na		
Folkestone Beds, 1½ in. below base of Gault, Copt Point, Folkestone, Kent	dark green pellets	10D	g, q, c, f, cl	g
Folkestone Beds, Sandling, Kent (sample FG1 of Padgham, 1970)	large olive green lumps	24L	g, cl	g, q
	dark olive pellets	24D	g, cl	g
Upper Greensand				
Gault, Glauconite bed of Bed XII, Abbots Cliff, Folkestone (1915 slip), base of bed	small dark green pellets	17D	g, mi	g
	small light green lumps	17L	g or m	g, c, q
Gault, Glauconite bed of Bed XII, Abbots Cliff, Folkestone (1915 slip), just above base	small dark green pellets	16D	g	g
	rare light green lumps	16L	cl	g, c, q
Gault, Glauconite bed of Bed XII, Abbots Cliff, Folkestone (1915 slip), near base of bed	small dark green pellets	15D	g, q	g
	rare light green lumps	15L	cl, q, f	g, c, q
Gault, Glauconite bed of Bed XII, Abbots Cliff, Folkestone (1915 slip), near top of bed	small dark green pellets	14D	g, cl	g
	small light green lumps	14L	g, q, c	g, q, c
Lower Chalk, Glauconitic Marl, Abbots Cliff, Folkestone (1975 exposure), near base	small dark green pellets	13D	g, mi, q, c, a	g, c
	small light green lumps	13L	cl, q, c	g, c, q
Lower Chalk, Glauconitic Marl, Abbots Cliff, Folkestone (1975 exposure), top of seam	small dark green pellets	12D	g, cl, q, f, a	g, c, q
	small light green lumps	12L	cl	g, c, q
Cambridge Greensand, Barrington, near Cambridge	0·5–0·2 mm pellets	18a	g, mi	g
	0·16–0·2 mm pellets	18b	g	g, c
Cambridge Greensand, Hauxton Road, Cambridge	dark green pellets	19D	g	g, c
	rare light green lumps	19L	g, mi	na
Lower Chalk, Glauconitic Marl, Glyndebourne Bore BDK 2792*, 48·3 m	dark green pellets	2D	g	na
	rare light green lumps	2L	cl	na
Eocene				
Upper Bracklesham Beds, Shepherds Gutter, Hampshire*	olive green pellets	21	g, mi	g, q, c
	dark green grains	—	q	na
Upper Bracklesham Beds, Kings Garn Gutter, Brook, Hampshire†	light and dark green pellets, some with iron stains	23L	g	g
Sea Floor Samples				
Mudstone, from 31° 33′ N. 10° 04·5′ W., 150 m (sample 873 of Summerhayes, 1971)	shiny, dark green grains	25D	mi, q	na
	light olive green grains	25L	g, cl	g
Phosphorite, from 31° 22′ N. 10° 16′ W., 400 m (sample 154 of Summerhayes, 1971)	black pellets	27L	g, q	g
	large green pellets	27	g	na
Glauconitic phosphatic conglomerate, 31° 21·5′ N. 10° 19·5′ W., 500 m (sample 155 of Summerhayes, 1971)	large dark green botryoidal pellets	29D	g, mi, a	g
Calcareous mudstone, from 31° 27′ N. 10° 24′ W. 750 m (sample 882 of Summerhayes, 1971)	light green pellets	34L	g, mi, c, f	na
	dark green pellets	34D	g, mi, a	g
Glauconitic phosphatic conglomerate, 31° 11·3′ N. 10° 04′ W., 150 m (sample 833 of Summerhayes, 1971)	light olive pellets	35L	g, mi	g, c
Silty limestone, from 31° 11·2′ N. 10° 06′ W., 140 m (sample 834 of Summerhayes, 1971)	light olive pellets	36	mi, c	g, c
DSDP 25-246-11-2, 24–5 cm from 33° 37′ S. 45° 09′ E., 1030 m, on Madagascar Ridge	green casts of foraminifera	—	m, c, mi	na

g = glauconite, m = montmorillonite, mi = mixed layer clays, cl = other clays, i = illite, q = quartz, c = calcite, f = feldspar, go = goethite staining, p = plagioclase, a = apatite, D = dark green pellets, L = light green lumps, (rare), na = not analysed, nd = not determined.

* Samples provided by permission of The Director, Institute of Geological Sciences.

† Samples provided by A. J. Fleet.

Potassium-argon dates: for 27L 49 Ma, 29D 14·4 Ma, 34L and D 13·1 Ma, 35L 10·6 Ma, from Summerhayes (1970).

DSDP samples provided by the Deep Sea Drilling Project.

The continental celadonites were separated from the host rock by crushing, after which the mineral could be readily hand picked from the debris. The ocean-floor basalts contain thin veins of celadonite from which the mineral can be picked using a sharp needle. Most of the celadonites appear to be homogenous when viewed through a binocular microscope (× 100), although small, glassy, white crystals of a zeolite (probably thomsonite) could be seen in part of BM 1907, 662, and sample DSDP 17-170-16-1, 24-6 cm, contains both light (A', Table IV) and dark (A) green celadonite in a vein. After the samples had been polished for EPMA, however, considerable surface variation due to inhomogeneity could be seen.

It was noted that after gentle grinding in an agate mortar and pestle in preparation for XRD analysis, the two minerals displayed marked colour differences: the celadonites exhibited a distinctly blue-green colour, whilst the glauconites were grassy-green and notably softer.

Microstructure. Several continental glauconite grains and celadonites from the ocean-floor basalts were examined by a scanning electron microscope (SEM) to see if any differences in the crystalline form of the minerals could be observed. Celadonite 'B', found growing in free space in a vesicle, forms radiating clusters of needles (fig. 1A); smectite from the same vesicle forms shorter blade-like radiating crystals (fig. 1B). No mixing of the two types was observed and the radial nature of both minerals persisted in material that did not grow into free space but formed veins.

Some glauconite pellets appear to be composed of numerous platy crystals, which often show a swirling foliation (fig. 1C), while other crystals exhibit a more or less ordered appearance (fig. 1D), and are similar to features described by Odin

TABLE II. *Location, description and analysis of celadonite samples*

Sample locality	Description	No.	XRD analysis	IR analysis
DSDP* 17-170-16-1, 24-6 cm 11° 48′ N. 177° 37′ E., 5792 m	green vein in basalt	A	cl, m, q	cl
DSDP* 25-249-33 cc 29° 56′ S. 36° 04′ E., 2088 m	green vesicles in basalt	B	cl, m, a, q	cl, s
DSDP*17-164-27-1, 107–10 cm 13° 12·14′ N. 161° 30·98′ W., 5499 m	mineral in crack in basalt	C	m, cl, c	c, cl
DSDP* 15-151-13-2, 67-8 cm 15° 01′ N. 73° 24′ W., 2029 m	green mud	—	m, c, q, f, cl, cy	cl silicates
DSDP* 17-166-29-3, 89-90 cm 03° 45′ N. 175° 04′ W., 4962 m	dark green mineral in basalt	—	m, i	no cl
DSDP* 17-167-95-2, 95-6 cm 07° 04′ N. 176° 49′ W., 3176 m	dark green mineral in breccia	—	m, f, a, q	c, cl, silicates
DSDP* 17-169-11-1, 87-9 cm 10° 40′ N. 173° 33′ E., 5407 m	mineral in cracks in basalt	—	m, cl, f, c	cl 5%, c, silicates
DSDP* 17-171-27-1, 128-31 cm 19° 07′ N. 169° 27′ W., 2290 m	green mineral in inter-pillow voids	—	tridymite	na
DSDP* 26-250A-1, 135 cm 33° 27′ S. 39° 22′ E., 5119 m	green mineral in basalt	—	cl, m	na
BM 89820, unknown locality	massive	D	cl	cl
BM 1907, 662 Thorshaven, Strømø, Faeroes	nodules	E	cl	cl
BM 1921, 223 Brentonico, Verona, Italy	massive	F	cl	cl
BM 1922, 973 Omaru District, New Zealand	massive	G	cl	cl
BM 1913, 333 Hall, Iceland	earthy, massive	H	cl, m	cl
BM 1948, 18 Truckee River, Washoe Co., Nevada	massive, in basalt	I	cl, m	cl, s
BM 32691 Monte Baldo, Verona, Italy	crystals in tuff	—	cl, q, m, cy	cl, q, ch
BM 89821 Marcano, Tyrol, Italy	crystals in matrix	—	cl, q, p, cy	cl, p
BM 1399 Val di Fassa, Italy	pseudomorphs after augite	—	cl, cy, m	cl
BM 1400 Val di Fassa, Italy	crystals in porphyry	—	cl, c, q	cl, c, q
BM 32709 Most, Bohemia	massive	—	g, mi, q	cl
BM 1937, 195 Buffaure, Val di Fassa, Italy	pseudomorphs after augite	—	cl, mi, ch	cl, ch, c, q
BM 1937, 1388 Guarapuara, Parana, Brazil	cavities in basalt	—	cl, ch, c, q, f	cl, ch, q

cl = celadonite, g = glauconite, i = illite, cy = other clays, s = saponite, ch = chlorite, m = montmorillonite, c = calcite, q = quartz, f = feldspar, a = amphibole, na = not analysed.

* Samples provided by the Deep Sea Drilling Project.

(1975). These are not always visible on the surface of a pellet since a covering, presumably also of glauconitic material, is sometimes present. This may be similar to the corona described by Zumpe (1971) and Odom (1976), although major chemical differences between 'corona' and core were not revealed by EPMA.

Results of individual analytical methods

XRD analysis. All the samples were examined by XRD as a preliminary to further work. The initial results are shown in Tables I and II where the impurities are also listed. Discrepancies between these results and those from IR analyses are caused by the larger sample used for XRD. All the celadonites have sharp basal and *hkl* reflections (fig. 2) indicating a 1*M* type structure, while the glauconites gave broader basal reflections and reduced *hkl* reflections, indicating a 1*Md* type structure (fig. 2), and enabling differentiation between the two minerals to be made. These findings are in agreement with those of Carroll (1970). The measurement of basal spacings for clay mineral differentiation is unreliable when mixed-layering is present;

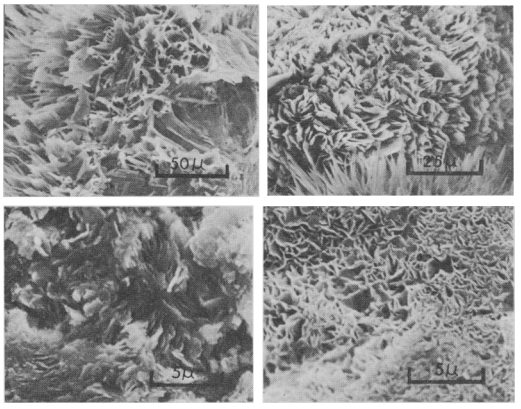

FIG. 1. Scanning electron microscope photographs of: (A) celadonite; (B) smectite, both from the vesicle in specimen 'B'; (C) part of the surface of a glauconite grain showing the crystal orientation; (D) a different surface texture on the same grain (from sample 10D).

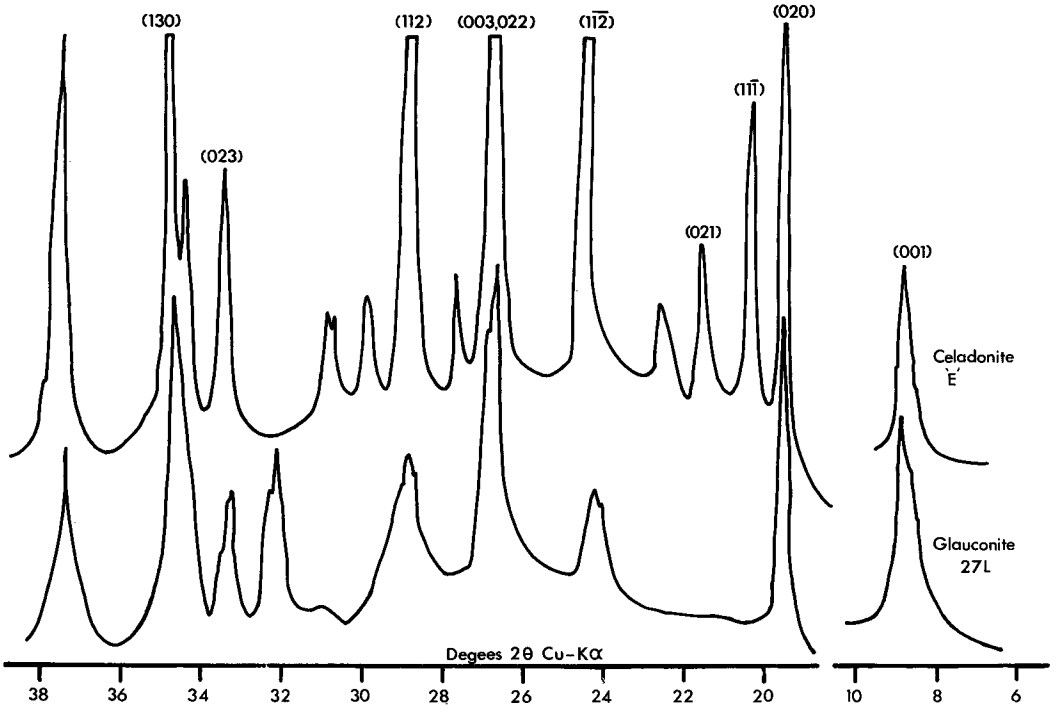

FIG. 2. XRD traces showing the characteristic peaks of glauconite 27L and celadonite E.

the *d* 060 spacings can, however, be used to distinguish between celadonites and glauconites, particularly when used in conjunction with the Fe^{3+} content of the unit cell (fig. 3).

IR analysis. Samples were pre-ground under alcohol and then incorporated in KBr discs as described by Russell (1974). Spectra were recorded over the range 4000–250 cm^{-1} in a Perkin Elmer 577 spectrometer. For all but one sample, celadonites were clearly distinguishable from glauconites by their spectra, and samples of the infra-red spectra of these two minerals are given in fig. 4. Celadonites exhibit extremely sharp absorption bands throughout their spectra, in which two to four narrow OH stretching bands are clearly resolved in the 3610–3530 cm^{-1} region, whereas glauconites give much broader absorption bands in which no more than three maxima can be poorly resolved in the region of OH stretching. A further point of distinction is that the band associated with an OH bending vibration, lying at 800 cm^{-1} in celadonites, is either entirely shifted to 815 cm^{-1} or partially displaced to give a doublet in glauconites. The sole exception, BM 32709, has a spectrum with the sharp absorption bands of celadonites, but exhibits a doublet at 810–815 cm^{-1}. The greater sharpness of the celadonite spectra reflects their more highly ordered structure within their individual layers, associated with the very low extent of substitution of Al for Si in the tetrahedral layer (Table IV) and the regular distribution of divalent and trivalent ions in the octahedral layer. The 815 cm^{-1} band of glauconites arises from Fe_2^{3+} OH groups, which are normally absent from celadonites. The exception BM 32709 is a mixed-layer celadonite–nontronite.

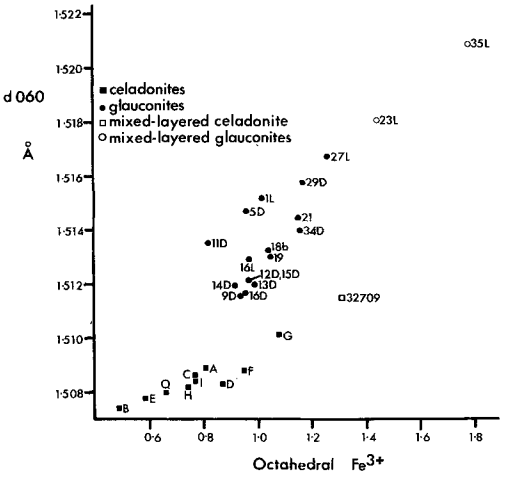

FIG. 3. Relationship of *d* 060 spacing to Fe^{3+} ions.

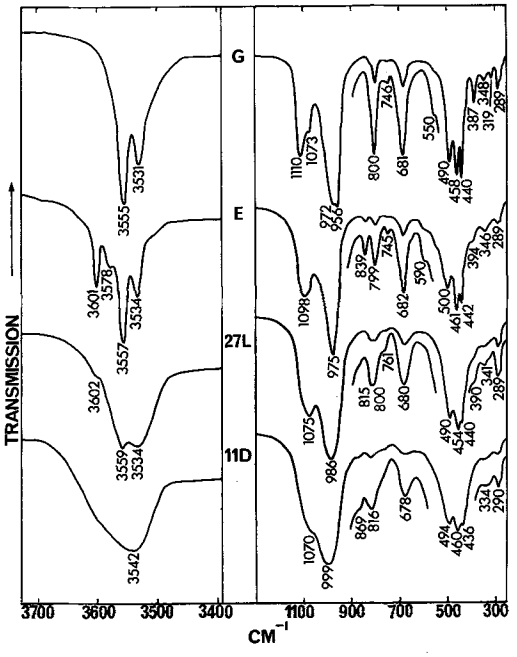

FIG. 4. Infra-red spectra of celadonites G and E, and glauconites 27L and 11D, illustrating the extremes of spectral sharpness and diffuseness found within each species of mica.

EPMA electron probe micro-analysis. The grains to be examined were set in resin in perspex mounts, ground by hand using wet and dry silicon carbide paper laps with paraffin lubricant, and polished by hand on paper laps with oil-based diamond pastes and lubricants. After polishing, the mounts were cleansed in diethyl ether, transferred in groups of nine to a brass specimen holder, and coated using a carbon beam evaporator. The specimens were analysed using a Cambridge Instruments' 'Geoscan' microprobe with an accelerating voltage of 15 kV and a specimen current of approximately 0·6 $\times 10^{-7}$ A. The standards used were independently analysed minerals, and the results were corrected using the method outlined by Sweatman and Long (1969), using the BM–IC–NPL computer program (Mason *et al.*, 1969). With each nine-specimen, eight-element analysis, an independent mineral standard, Kakanui augite (Mason, 1966; Mason and Allen, 1973) was run. Each specimen was analysed separately by two operators, each examining different grains. A minimum of six points on each grain were analysed, taking two ten-second counts on each spot. Inhomogeneous specimens were analysed after first determining the areas of celadonite or glauconite, using potassium content

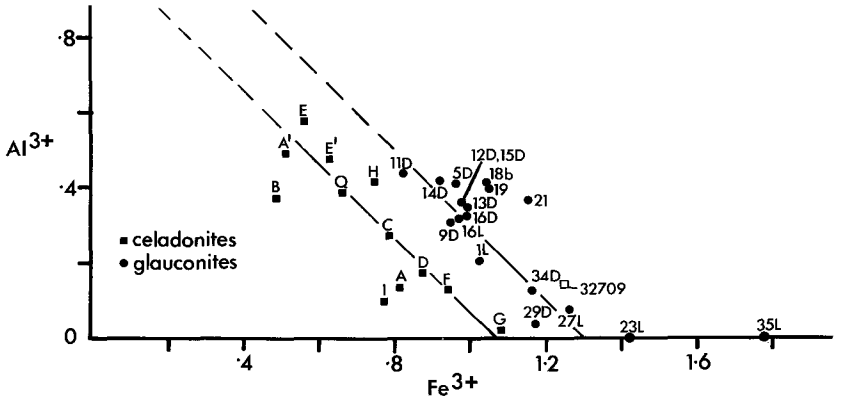

FIG. 5. Relationship between the number of octahedral Al ions and trivalent Fe ions per half unit cell from the EPMA analyses. Dashed lines indicate the position of the average R^{3+} content of 1·04 for celadonites and 1·34 for glauconites. Sample 32709 is a mixed-layered celadonite, 23L and 25L are mixed-layered glauconites.

as a guide. Since the 'Geoscan' has two spectrometers enabling two elements to be determined simultaneously iron and potassium were first analysed together followed by analysis for magnesium and again, iron, which ensured that the correct area was being examined. Since none of the ferruginous impurities present were known to contain major potassium, this method is considered valid for the samples studied. It is assumed that all the H_2O^- was driven off by the electron beam; the low totals of some analyses (Tables III and IV) may be due to the effects of imperfect polish on the specimens, in particular those with an 'L' suffix.

The extent of compositional variation within a sample of celadonite is shown by the analyses of E and E′ and A and A′. In the latter pair there is considerable octahedral Fe^{3+}–Al^{3+} reciprocal variation although the total trivalent octahedral occupancy remains constant (fig. 5). Element distribution photographs taken of this specimen by EPMA show the potassium to have an even distribution over a wide area while aluminium and iron show a reciprocal relationship. There is a sharp boundary between the two celadonites in some areas (fig. 6), while in others the one grades into the other. Areas of the A′ celadonite can be seen to have slightly higher Mg contents than the rest, which is in agreement with chemical analyses obtained for other samples of A and A′. Celadonite A′ also has a much smaller *d* 060 spacing (1·5065 Å) compared with other members of this species.

XRF and wet chemistry. Five samples analysed by EPMA were re-analysed by XRF (Tables III and IV) in order to confirm the results. The samples were prepared by fusing with lithium metaborate (1:4) and analysed as pressed glass discs using international standards prepared in the same way for comparison. The analyses compare closely with

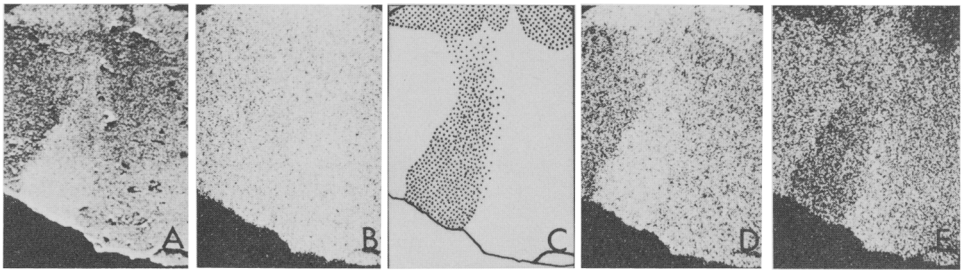

FIG. 6. EPMA photographs of samples A and A^1 showing (A) backscattered electrons, (B) potassium distribution, (C) distribution of dark green celadonite type A (stippled) and light blue-green celadonite type A^1 (plain), (D) distribution of iron and (E) distribution of aluminium.

TABLE III. *Electron probe microanalyses and structural formulae of glauconites*

	1	5	9D	11D	12D	13D	14D	14D*	15D	16D	16L
SiO_2	39·77	49·47	51·53	51·45	51·36	51·12	52·87	49·90	52·39	51·51	52·80
TiO_2	0·55	0·04	0·05	0·02	0·00	0·00	0·04	0·06	0·04	0·00	0·09
Al_2O_3	6·12	9·32	6·24	7·19	6·90	6·71	7·87	7·80	7·32	6·25	7·68
Fe_2O_3	15·16	17·37	17·27	14·81	17·73	17·91	17·14	15·60	18·14	17·68	17·98
FeO	8·52	6·98	5·98	8·28	3·47	3·43	4·37	2·70	3·99	4·15	3·80
MnO	nd	nd	nd	nd	nd	nd	nd	0·01	nd	nd	nd
MgO	1·98	2·61	3·88	2·72	4·18	4·09	4·30	4·40	4·21	4·08	3·69
CaO	0·28	0·73	0·52	0·23	0·31	0·62	0·40	2·20	0·32	0·23	0·43
Na_2O	0·64	0·00	0·02	0·00	0·07	0·03	0·03	0·08	0·00	0·02	0·05
K_2O	5·48	7·60	8·13	8·12	8·38	8·41	8·37	8·18	8·84	8·48	7·72
H_2O+	nd	nd	nd	nd	nd	nd	nd	5·35	nd	nd	nd
P_2O_5	nd	nd	nd	nd	nd	nd	nd	1·18	nd	nd	nd
CO_2	nd	nd	nd	nd	nd	nd	nd	0·54	nd	nd	nd
Total	78·50	94·12	93·62	92·82	92·40	92·32	95·39	98·00	95·25	92·40	94·24
Numbers of ions on the basis of 22 (O,OH,F)											
Si	3·57	3·62	3·77	3·81	3·77	3·77	3·76	3·77	3·75	3·79	3·77
Al	0·43	0·38	0·23	0·19	0·23	0·23	0·24	0·23	0·25	0·21	0·23
Al	0·21	0·42	0·31	0·44	0·36	0·35	0·42	0·46	0·36	0·33	0·32
Fe^{3+}	1·02	0·96	0·95	0·82	0·98	0·99	0·92	0·88	0·98	0·99	0·97
Fe^{2+}	0·64	0·43	0·37	0·51	0·21	0·21	0·26	0·17	0·24	0·26	0·23
Mg	0·26	0·28	0·42	0·30	0·46	0·45	0·45	0·49	0·45	0·45	0·39
Ti	0·04	0·00	0·00	0·01	0·00	0·00	0·00	0·00	0·00	0·00	0·01
Ca	0·05	0·11	0·08	0·04	0·05	0·09	0·06	0·06	0·05	0·04	0·06
Na	0·11	0·00	0·00	0·00	0·01	0·00	0·00	0·01	0·00	0·00	0·00
K	0·62	0·71	0·76	0·76	0·79	0·79	0·76	0·78	0·81	0·80	0·70
$\Sigma R^{3+}R^{2+}$	2·17	2·09	2·05	2·08	2·01	2·00	2·05	2·00	2·03	2·03	1·92
ΣR^{3+}	1·23	1·38	1·26	1·26	1·34	1·34	1·34	1·34	1·34	1·32	1·29
ΣA	0·78	0·82	0·84	0·80	0·85	0·88	0·82	0·85	0·86	0·84	0·76

	18b	18b*	19	21	23L	27L	29D	34D	34D*	35L	35L*
SiO_2	51·95	49·70	52·00	49·11	37·20	47·43	50·12	50·64	49·50	48·05	45·30
TiO_2	0·07	0·10	0·02	0·04	0·05	0·05	0·02	0·04	0·08	0·05	0·15
Al_2O_3	8·87	9·30	8·55	9·41	5·81	4·25	2·41	3·45	3·50	2·22	4·30
Fe_2O_3	19·65	16·50	19·62	21·00	21·10	21·60	20·33	20·37	21·20	31·92	24·40
FeO	2·98	2·20	2·58	2·71	8·04	1·78	2·07	2·49	2·50	1·59	1·10
MnO	nd	0·02	nd	nd	nd	nd	nd	nd	0·01	nd	0·01
MgO	3·71	4·00	3·84	3·06	2·18	4·72	6·35	5·32	4·90	3·87	3·90
CaO	0·68	1·32	0·65	0·35	0·57	0·45	0·16	0·17	1·16	0·40	4·06
Na_2O	0·01	2·19	0·00	0·03	0·00	0·25	0·02	0·03	0·13	0·19	0·30
K_2O	8·23	7·85	8·23	8·68	5·55	8·31	8·19	8·15	8·58	6·86	4·84
H_2O+	nd	5·32	nd	nd	nd	nd	nd	nd	5·69	nd	8·35
P_2O_5	nd	0·43	nd	nd	nd	nd	nd	nd	0·61	nd	0·25
CO_2	nd	0·40	nd	nd	nd	nd	nd	nd	0·59	nd	3·83
Total	96·15	99·33	95·49	94·39	80·50	88·84	89·67	90·66	98·45	95·15	100·79
Numbers of ions on the basis of 22 (O,OH,F)											
Si	3·67	3·65	3·69	3·57	3·34	3·69	3·83	3·82	3·81	3·57	3·69
Al	0·33	0·35	0·31	0·43	0·61	0·31	0·17	0·18	0·19	0·19	0·31
Al	0·41	0·45	0·40	0·37	0·00	0·08	0·04	0·13	0·13	0·00	0·10
Fe^{3+}	1·04	0·91	1·05	1·15	1·42	1·26	1·17	1·16	1·23	1·78	1·49
Fe^{2+}	0·17	0·13	0·15	0·17	0·60	0·12	0·13	0·16	0·16	0·09	0·07
Mg	0·39	0·44	0·41	0·33	0·29	0·55	0·72	0·60	0·55	0·43	0·38
Ti	0·00	0·00	0·00	0·00	0·00	0·00	0·00	0·00	0·00	0·00	0·00
Ca	0·10	0·06	0·09	0·05	0·11	0·07	0·03	0·03	0·00	0·06	0·00
Na	0·00	0·31	0·00	0·00	0·00	0·04	0·00	0·00	0·01	0·03	0·05
K	0·74	0·73	0·74	0·80	0·63	0·82	0·79	0·78	0·84	0·65	0·50
$\Sigma R^{3+}R^{2+}$	2·01	1·93	2·01	2·02	2·31	2·01	2·06	2·05	2·07	2·30	2·04
ΣR^{3+}	1·45	1·36	1·45	1·51	1·42	1·34	1·21	1·29	1·36	1·78	1·59
ΣA	0·84	1·10	0·83	0·85	0·74	0·93	0·82	0·81	0·85	0·74	0·55

nd = not determined; in structural formula, P_2O_5 deducted as $Ca_5(PO_4)_3OH$; CaO and CO_2 as $CaCO_3$.

* Additional analysis by XRF (analyst G. C. Jones), with CO_2 and H_2O determined by CHN analyser (analyst G. C. Jones) and Fe^{3+}/Fe^{2+} determined by V. K. Din and A. J. Easton.

Analysts J. C. Bevan and K. M. Brown.

TABLE IV. *Electron probe microanalyses and structural formulae of celadonites*

	A	A′	B	C	D	D*	E	E′	F	G	H	I	Q	BM 32709*	BM 32709
SiO_2	54·84	53·64	52·27	52·58	53·40	53·00	56·05	54·14	50·51	52·28	47·43	47·23	55·80	49·70	52·31
TiO_2	0·00	nd	0·00	0·20	0·04	0·27	0·04	0·00	0·00	0·00	0·04	0·00	0·29	0·38	0·26
Al_2O_3	1·69	5·85	4·17	5·28	2·51	2·90	6·88	6·38	1·40	0·82	4·21	2·87	5·76	1·90	2·15
Fe_2O_3	14·81	9·14	8·80	14·61	15·88	16·40	10·30	11·57	15·90	18·99	11·75	12·67	12·28	21·90	21·82
FeO	5·88	3·28	5·39	3·37	3·53	3·80	3·98	4·47	3·94	3·02	3·68	2·81	3·39	2·30	2·07
MnO	nd	nd	nd	nd	nd	0·02	nd	nd	nd	nd	nd	nd	nd	0·02	nd
MgO	6·98	7·94	6·06	6·35	6·45	6·20	4·95	5·71	5·45	6·33	4·28	9·00	6·78	3·70	3·34
CaO	0·07	0·12	0·07	0·68	0·07	0·33	0·22	0·04	0·10	0·16	0·31	0·39	0·36	1·95	1·04
Na_2O	0·15	nd	0·02	0·31	0·05	0·38	0·05	0·00	0·02	0·00	0·03	0·00	0·81	0·02	0·00
K_2O	8·93	8·97	8·20	7·69	10·28	9·38	10·29	9·89	8·75	9·43	8·26	8·57	9·28	6·65	6·72
H_2O+	nd	nd	nd	nd	nd	4·59	nd	nd	nd	nd	nd	nd	nd	5·78	nd
P_2O_5	nd	nd	nd	nd	nd	0·10	nd	nd	nd	nd	nd	nd	nd	0·09	nd
CO_2	nd	nd	nd	nd	nd	0·75	nd	nd	nd	nd	nd	nd	nd	4·00	nd
Total	93·35	88·94	84·98	91·07	92·21	98·12	92·76	92·20	86·07	91·03	79·99	83·54	94·75	98·39	89·71
Numbers of ions on the basis of 22 (O,OH,F)															
Si	4·01	3·98	4·09	3·83	3·96	3·94	4·01	3·94	4·01	3·95	3·99	3·83	3·91	3·92	3·95
Al	0·00	0·02	0·00	0·17	0·04	0·06	0·00	0·06	0·00	0·05	0·01	0·17	0·09	0·08	0·05
Al	0·15	0·49	0·38	0·28	0·18	0·19	0·58	0·48	0·13	0·02	0·41	0·10	0·39	0·10	0·15
Fe^{3+}	0·81	0·51	0·49	0·78	0·87	0·92	0·56	0·63	0·95	1·08	0·75	0·77	0·66	1·30	1·24
Fe^{2+}	0·39	0·20	0·37	0·22	0·24	0·24	0·24	0·27	0·26	0·19	0·25	0·19	0·20	0·15	0·13
Mg	0·75	0·88	0·71	0·69	0·71	0·63	0·53	0·62	0·64	0·71	0·45	1·08	0·72	0·41	0·37
Ti	0·00	nd	0·00	0·01	0·00	0·01	0·00	0·00	0·00	0·00	0·00	0·00	0·01	0·02	0·01
Ca	0·01	0·01	0·00	0·10	0·01	0·00	0·03	0·00	0·01	0·03	0·05	0·06	0·06	0·00	0·16
Na	0·02	0·00	0·00	0·04	0·00	0·05	0·00	0·00	0·00	0·00	0·00	0·00	0·11	0·00	0·00
K	0·83	0·85	0·82	0·73	0·97	0·89	0·94	0·92	0·88	0·91	0·88	0·88	0·85	0·67	0·65
$\Sigma R^{3+}R^{2+}$	2·10	2·08	1·95	1·98	2·00	1·98	1·91	2·00	1·98	2·00	1·86	2·14	1·98	1·98	1·90
ΣR^{3+}	0·96	1·00	0·87	1·06	1·05	1·11	1·14	1·11	1·08	1·10	1·16	0·87	1·05	1·40	1·39
ΣA	0·86	0·86	0·82	0·87	0·97	0·89	0·97	0·92	0·89	0·94	0·93	0·94	1·02	0·67	0·81

nd = not determined; in structural formula, P_2O_5 deducted as $Ca_5(PO_4)_3OH$; CaO and CO_2 as $CaCO_3$.

* Additional analysis by XRF (analyst G. C. Jones), with CO_2 and H_2O determined by CHN analyser (analyst G. C. Jones) and Fe^{3+}/Fe^{2+} determined by V. K. Din and A. J. Easton.

Analysts J. C. Bevan and K. M. Brown.

Sample A contains light blue-green mineral A′ grading into green mineral A.

Sample E is divided into E (matrix) and E′ (smooth areas in the matrix).

BM 32709 is a mixed layer celadonite–nontronite.

Sample Q is a re-analysis of Kempe (1974).

the EPMA results with the exception of 35L, which is a mixed-layer species. The Fe^{2+}/Fe^{3+} ratio was determined using a modification (Easton, 1972) of the ferrous 2,2′-dipyridyl iron complex (Riley and Williams, 1959). This ratio was then applied to the total iron determined by microprobe.

Discussion

The conventional distinction between glauconite and celadonite, based on mode of origin, is to a large extent reflected in certain features of chemical composition, X-ray diffraction pattern, infra-red spectra, and crystal morphology of the samples examined here; taken together, these features distinguish unambiguously celadonites from glauconites.

The essential differences are revealed by the chemical analysis, and in particular by the half unit cell contents (Tables III and IV, fig. 5). The total number of octahedral trivalent atoms per half unit cell (R^{3+}) is constant for each species, being on average 1·04 for celadonites and 1·34 for glauconites, but within these limits considerable variation in the amounts of Al^{vi} and Fe^{3+} exists (fig. 5), although Fe^{3+} remains predominant. Further, celadonites show less Al tetrahedral substitution; thirteen of the fifteen analysed celadonites have fewer than 0·1 Al^{3+} ions per four tetrahedral sites, while the remaining two samples (C and I) fall just on the lower limit (0·17) of the glauconite field (0·17–0·61 Al^{3+}).

The average R^{3+} determined for glauconites and celadonites from the current analyses is lower than that found by previous workers. The average R^{3+} of 1·48 for glauconites is calculated from the results of Odom (1976), Foster (1969), Thompson and Hower (1975), Bentnor and Kastner (1965), Hendricks and Ross (1941), and Weaver and Pollard (1973). The average R^{3+} for celadonites calculated

from the results of Foster (1969), Wise and Eugster (1964), Hendricks and Ross (1941), and Kohyama *et al.* (1971) is 1·15. These samples plot along lines parallel to the current results (fig. 5) and show a similar degree of Al^{vi}–Fe^{3+} substitution. The reason for the difference is uncertain: the fact that the earlier work was done by bulk wet-chemical analysis may be a contributory factor. EPMA work by Kastner (1976) on a celadonite from DSDP basalt sample 323-19-3, 90–2 cm, gave a R^{3+} value of 1·03 when the average celadonite Fe^{3+}/Fe^{2+} ratio of 2·6 from the current work was applied and is in line with the present results rather than those of previous workers. A strong correlation was found for both glauconite and celadonite between the Fe^{3+} content and the *d* 060 spacing (fig. 3), the former having a *d* 060 greater than 1·51 Å, the latter less than 1·51 Å.

Exceptions to the above generalizations fall into three groups: 23L and 35L; BM 32709; and 1L, 5D, and 11D. The first group consists of mixed layer glauconite–smectites (about 10 and 25% mixed-layering respectively) and were included in order to illustrate the abnormal trends that mixed-layering induces. Figs. 3 and 5 show their octahedral Fe^{3+} content and *d* 060 spacing to be much greater than in the pure minerals. Of the second type, BM 32709 was at first thought to be a mixed-layer glauconite–smectite from the XRD trace, while the IR data indicated that it was a mixed-layer celadonite. This is supported by its position on figs. 3 and 5 where it shows trends away from the pure celadonites similar to those shown by 23L and 35L relative to pure glauconites. In addition, all the mixed-layer species show considerably higher total octahedral occupancies than the norm for glauconites and celadonites. The third group differ from the others in an altogether different respect. These samples have the morphology and IR and XRD patterns of glauconites, but have higher Fe^{2+} and lower Mg contents than normal. The environment from which 11D was extracted was very much reduced, containing pyrite and free sulphur; 1L and 5D are from the same bed but from inland boreholes. It is suspected that these samples were initially 'normal' glauconite but have since undergone considerable reduction.

From the data available it appears that glauconites from different outcrops in the same area and geological horizon have similar compositions. The glauconites from the Lower and Upper Greensand plot separately, as do the Moroccan continental shelf deposits. There also seems to be a loss of Fe^{3+} and Mg and a corresponding gain of Al and Fe^{2+} with increasing age: oceanic glauconites also show higher oxidation states.

Conclusions

1. Celadonites and glauconites form separate mineral species: within each group considerable chemical variation can be found. A rough distinction between them can be made from their overall bulk chemical analysis, celadonites usually having higher MgO and K_2O but lower total Fe_2O_3 than glauconites. Further, each of the two minerals is an individual isomorphous replacement series, celadonites approaching the ideal half unit cell of the type: $K(Fe^{3+}, Al^{3+})(Mg^{2+}, Fe^{2+})Si_4O_{10}(OH)_2$, whilst the glauconites have an average half unit cell of the type: $K_{0.85}(Fe^{3+}, Al^{3+})_{1.34}(Mg^{2+}, Fe^{2+})_{0.66}(Si_{3.76}, Al_{0.24})O_{10}(OH)_2$. In the latter the divergence of the octahedral layer from the optimum $R^{3+}R^{2+}$ ratio of 1:1 and the considerable substitution of aluminium in the tetrahedral layer presumably leads to the relative disorder within the layers of this structure and a lower energy of formation.

2. Celadonites and glauconites can be differentiated readily by both IR and XRD: in the case of the latter, particularly so when the *d* 060 spacings are plotted against the ferric iron content of the half unit cell (fig. 3).

3. An apparent systematic discrepancy between chemical data as determined by EPMA and bulk 'wet' chemical methods was noted, the cause of which is not known. This results in lower Al_2O_3 and R^{3+} occupancy in the present data than in that previously reported.

4. Glauconites from a given geological horizon generally have a similar composition, whereas celadonites may show a wide range of composition within the same bulk sample.

5. The term 'glauconite' or 'glauconitic' has been used in several contexts: to describe glauconite-bearing sediments; for individual grains or pellets containing glauconite; or to denote a specific mineral species (McRae, 1972). Some authors (e.g. Thompson and Hower, 1975) refer to the mixed-layer minerals, which consist of interstratified layers of glauconite and smectite, as 'glauconite' even though it may be the minor constituent. On the basis of the results reported here it is suggested that the term 'glauconite' be reserved for use in the specific mineralogical sense; that both constituents be specified in naming mixed-layer clays; and that the adjective 'glauconitic' be used in all other contexts.

Acknowledgements. Thanks are due to the Deep-Sea Drilling Project and National Science Foundation, the Director of the Institute of Geological Sciences, London, and Dr. A. J. Fleet of the Open University for providing some of the samples used in this study. The authors would

like to thank Dr. D. R. C. Kempe of the British Museum (Natural History) for critically reading this manuscript and his editorial comments.

REFERENCES

Bentnor (Y. K.) and Kastner (M.), 1965. *Jour. Geol. Petr.* **35,** 155–66.

Carroll (D.), 1970. *Geol. Soc. Am. Spec. Pap.* **126,** 1–80.

Easton (A. J.), 1972. *Chemical analysis of silicate rocks,* 1–258, Elsevier, London.

Foster (M. D.), 1969. *U.S. Geol. Surv. Prof. Pap.* **614-F,** 1–17.

Hendricks (S. B.) and Ross (C. S.), 1941. *Am. Mineral.* **26,** 683–708.

Kastner (M.), 1976. In Schlanger (S. O.) and Johnson (E. D.), *Initial Reports Deep-Sea Drilling Project,* **35,** 518–19.

Kempe (D. R. C.), 1974. In Davis (T. A.) and Luyendyk (B. P.), Ibid. **26,** 465–503.

Kohyama (N.), Shimode (S.), and Sudo (T.), 1971. *Mineral. J. Japan,* **6,** 299–312.

Mason (B.), 1966. *N.Z. J. Geophys.* **9,** 474–80.

—— and Allen (R. O.), 1973. *N.Z. J. Geophys.* **16,** 935–47.

Mason (P.), Frost (M. T.), and Reed (S. J. B.), 1969. *National Physical Lab. I.M.S. Report 1.*

McRae (S. G.), 1972. *Earth-Sci. Rev.* **8,** 397–440.

Odin (G. S.), 1975. Ph.D. Thesis, Univ. P. et M. Curie de Paris.

Odom (I. E.), 1976. *Clays Clay Miner.* **24,** 232–8.

Padgham (R. C.), 1970. Unpublished Ph.D. Thesis, Univ. of London.

Riley (J. P.) and Williams (M. P.), 1959. *Mikrochim. Acta,* **4,** 516–24.

Russell (J. D.), 1974. In Farmer (V. C.), *The infra-red spectra of minerals,* Min. Soc. Lond., 11–25.

Summerhayes (C. P.), 1970. Unpublished Ph.D. Thesis, Univ. of London.

Sweatman (T. R.) and Long (J. V. P.), 1969. *J. Petrol.* **10,** 332–76.

Thompson (G. R.) and Hower (J.), 1975. *Clays Clay Miner.* **23,** 289–300.

Weaver (C. E.) and Pollard (L. D.), 1973. *The chemistry of clay minerals,* Elsevier, 23–45.

Wise (S. E.) and Eugster (H. P.), 1964. *Am. Mineral.* **49,** 1031–83.

Zumpe (H. H.), 1971. *Mineral. Mag.* **38,** 215–24.

[*Manuscript received 23 June 1977, revised 19 December 1977*]